A THREE-DIMENSIONAL STEADY-STATE TUMOR SYSTEM

WENRUI HAO[*], JONATHAN D. HAUENSTEIN[†], BEI HU[‡], AND ANDREW J. SOMMESE[§]

Abstract. The growth of tumors can be modeled as a free boundary problem involving partial differential equations. We consider one such model and compute steady-state solutions for this model. These solutions include radially symmetric solutions where the free boundary is a sphere and nonradially symmetric solutions. Linear and nonlinear stability for these solutions are determined numerically.

Key words. Free boundary problems, stationary solution, stability, instability, bifurcation, discretization, condition number, Bertini, tumor growth.

AMS subject classifications. Primary 14Q99, 65M22, 35R35, 35K55; Secondary 35Q80, 35C20, 92C37.

1. The Model. We consider the free boundary problem modeling tumor growth that was studied in [12] and the references [1, 5, 6, 7, 8, 9, 10, 11, 13, 15, 16] therein.

Let $\Omega(t)$ denote the tumor domain at time t, and p the pressure within the tumor resulting from the proliferation of the tumor cells. The density of the cells, c, depends on the concentration of nutrients, σ, and, assuming that this dependence is linear, we simply identify c with σ. We also assume a linear dependence of the proliferation rate S on σ: $S = \mu(\sigma - \tilde{\sigma})$ $(\tilde{\sigma} > 0)$ where $\tilde{\sigma}$ is a threshold concentration and μ is a parameter expressing the "intensity" of the expansion by mitosis (if $\sigma > \tilde{\sigma}$) or shrinkage by apoptosis (if $\sigma < \tilde{\sigma}$) within the tumor. The function σ satisfies the diffusion equation:

$$\sigma_t - \Delta\sigma = -\sigma \qquad \text{in } \Omega(t). \tag{1.1}$$

The pressure p is related to the velocity $\vec{V}$ of the concentration σ, and, assuming Darcy's law in the tissue, we have $\vec{V} = -\nabla p$. Since, by conservation of mass, $\text{div}\vec{V} = S$, we obtain for the pressure p the equation

$$\Delta p = -\mu(\sigma - \tilde{\sigma}) \qquad \text{in } \Omega(t). \tag{1.2}$$

As in the papers cited above, σ and p satisfy the boundary conditions:

$$\sigma = 1 \qquad \text{on } \partial\Omega(t) \qquad (1 > \tilde{\sigma}), \tag{1.3}$$

$$p = \kappa \qquad \text{on } \partial\Omega(t) \tag{1.4}$$

where κ is the mean curvature ($\kappa > 0$ if $\Omega(t)$ is a ball). Furthermore,

$$V_n = -\frac{\partial p}{\partial n} \qquad \text{on } \partial\Omega(t) \tag{1.5}$$

where n is the outward normal and V_n is the velocity of the free boundary $\partial\Omega(t)$ in the direction n.

The model is summarized into the following reaction-diffusion system:

$$\begin{cases} \sigma_t - \Delta\sigma &= -\sigma & \text{in } \Omega(t) \\ -\Delta p &= \mu(\sigma - \tilde{\sigma}) & \text{in } \Omega(t) \\ \sigma &= 1 & \text{on } \partial\Omega(t) \\ p &= \kappa & \text{on } \partial\Omega(t) \\ \frac{\partial p}{\partial n} &= -V_n & \text{on } \partial\Omega(t). \end{cases} \tag{1.6}$$

The steady-state tumor model of (1.6) is thus given by

$$\begin{cases} -\Delta\sigma &= -\sigma & \text{in } \Omega \\ -\Delta p &= \mu(\sigma - \tilde{\sigma}) & \text{in } \Omega \\ \sigma &= 1 & \text{on } \partial\Omega \\ p &= \kappa & \text{on } \partial\Omega \\ \frac{\partial p}{\partial n} &= 0 & \text{on } \partial\Omega. \end{cases} \tag{1.7}$$

For the system (1.6) with smooth initial data, local existence and uniqueness was proved in [3, 4]. In [13] it was proved that for any $0 < \tilde{\sigma} < 1$ there exists a unique radially symmetric stationary solution, and its radius depends on $\tilde{\sigma}$, but not on μ. It is proved that for small μ, radially symmetric solutions are asymptotically stable. In [14] it was proved in the 2-dimensional case that there exists a sequence of symmetric-breaking branches of stationary solutions of (1.7) bifurcating from μ_n ($n = 2, 3, 4, \ldots$). A general simplified proof, which works also for the 3-dimensional case, was proved in [10]. The asymptotic stability of the spherical solution for $\mu < \mu_2$ and of the first bifurcation branch was studied extensively in [11, 12]; earlier results for small μ were established in [4].

There results imply, in particular, there exists a radially symmetric stationary solution with free boundary $r = R$ for any positive number R. Since tumors grown in vitro have a nearly spherical shape, it is important to determine whether these radially symmetric tumors are asymptotically stable.

While tumors grown in vitro have a nearly spherical shape, tumors grown in vivo are usually not. It is therefore also very interesting to study the behavior of non-radially symmetric tumors.

It was shown that the bifurcation points satisfies $\mu_2 < \mu_3 < \cdots$. It was shown in [11] that it is possible for the radially symmetric solution to change the stability at μ_2. Moreover, [12] showed that it is possible to have a branch of stable non-radially symmetric solutions near μ_2 and an unstable branch of non-radially symmetric
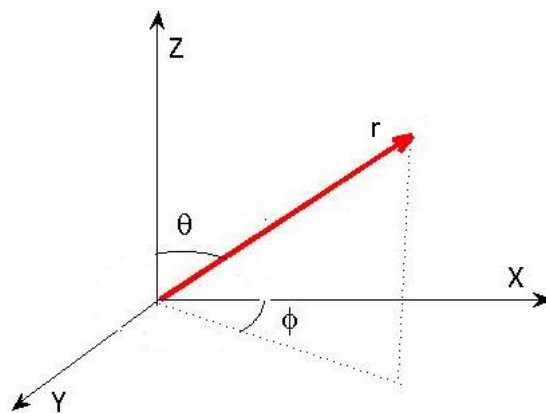
Fig. 2.1: Spherical polar coordinates

solutions also near μ_2. In particular, this shows that the non-radially symmetric solution branches near μ_2 are of particular interest.

Note that these results are valid only in a small neighborhood of the bifurcation branching point. A very challenging question is to find out what happens if the parameters *go beyond this small neighborhood.* It is clear that numerical computation is needed to answer these questions. In particular, it is interesting to find out whether it is possible for the tumor to grow into other shapes. This is the goal of this paper, by discretizing our system and tracking the condition number, we were able to track along the bifurcation branch well beyond the bifurcation point, and in the process we found a variety of possible shapes of steady state solutions. Some of these solutions are stable while some others are not. Our results are shown in Figures 3.3–3.6.

2. Discretization. We utilize spherical coordinates to discretize the system with the exception of the origin and Z-axis, which are singular. Any spherical coordinate triplet (r, θ, ϕ) showed in Figure 2 specifies a single point of three-dimensional space:

$$x = r\cos(\phi)\sin(\theta)$$
$$y = r\sin(\phi)\sin(\theta)$$
$$z = r\cos(\theta),$$

where

$$
\begin{array}{ccccc}
0 & \leq & r & < & \infty \\
0 & \leq & \theta & \leq & \pi \\
0 & \leq & \phi & < & 2\pi.
\end{array}
$$

We first consider the tumor model which is symmetrical in the ϕ direction. In this case, we just consider the model in the θ direction. We will discuss the model without such symmetry in section 4. To handle the free boundary, we developed a

Table 2.1: Errors and orders

Formula	value
$\max |x_{10} - x_{20}|$	$7.941387350995921 \times 10^{-6}$
$\max |x_{10} - x_{40}|$	$7.410376192340529 \times 10^{-6}$
$\max |x_{20} - x_{40}|$	$6.082857159639410 \times 10^{-7}$
$\max |x_{10} - x_{80}|$	$7.365667755276917 \times 10^{-6}$
$\max |x_{20} - x_{80}|$	$6.552861596662352 \times 10^{-7}$
$\max |x_{40} - x_{80}|$	$4.488189964124700 \times 10^{-8}$
$\log_2 \left(\frac{\|x_{10} - x_{80}\|_2}{\|x_{20} - x_{80}\|_2} \right)$	2.650665052445782
$\log_2 \left(\frac{\|x_{20} - x_{80}\|_2}{\|x_{40} - x_{80}\|_2} \right)$	2.747739401255624

novel discretization approach to allow the length of the grid to change in coordination with the boundary, i.e., let R_i be the length of tumor in the θ_i direction, which change independently and model the free boundary in that direction. In this case, we setup N_R equally spaced grid points between the origin and R_i in each direction. Let N_θ denote the number of grid points in the θ direction. Near the boundary, we add two additional grid points for improved accuracy that also change in accordance with the boundary. Figure 2.2 presents the grid points for a radial and nonradial solution with $N_\theta = 20$ and $N_R = 20$.

Using this grid, we apply the third order finite difference scheme to setup a discretization of the system (1.7) yielding a polynomial system. The variables of this polynomial system correspond to the location of the boundaries in each direction and the concentration of nutrients and pressure at each grid point. We check the convergence of the numerical solution of the system by doubling the number of grid points and quadrupling the number of grid points. In table 2.1, $x_{10 \times i}$ represents the solutions with $N_R = 10 \times i$, $N_\theta = 10 \times i$ respectively, where $i = 1, 2, 4, 8$. It shows that the numerical solution converges to the actual solution by increasing grid points.

3. Bifurcation Problem. As mentioned in Section 1, the system depends on the positive parameter μ and, for a sequence of values $\mu_2 < \mu_3 < \cdots$, there exists branches of symmetry breaking stationary solutions [10]. These solution branches extend beyond a small neighborhood of the bifurcation points along the branch of radially symmetry solutions. One goal of this paper is to compute the values of μ_n where these bifurcations occur.

Starting from a radially symmetric solution and using parameter continuation with respect to μ, we are able to track along the set of radially symmetric solutions of the discretized polynomial system for a given radius. At the values of μ where nonradially symmetric solution branches exist, the radially symmetric solution is singular, i.e., the Jacobian matrix of the non-symmetrized system is rank deficient. By monitoring the Jacobian matrix of the discretized polynomial system using parameter continuation, we can compute the values of $\mu_2, \mu_3, \ldots$ numerically.

By monitoring the "condition number," that is,

$$CN = \|J(x)\|\|J^{-1}(x)\| \tag{3.1}$$

where $J(x)$ is the Jacobian matrix evaluated at x, we can identify when the Jacobian matrix becomes rank deficient. In our tests, the error between the numerically computed values of μ_n, $2 \leq n \leq 10$, and the theoretic values is relatively small. For example, using a radius of 2.5, we numerically computed $\mu_2 = 4.043$ and $\mu_3 = 9.314$. The theoretical values are $\mu_2 = 4.042$ and $\mu_3 = 9.319$ [12]. Figure 3.1 plots the condition number with respect to μ as we track along the radially symmetric solution branch with radius 2.5 from $\mu = 3$ to $\mu = 10$. This plot clearly shows the two blows up that occur at μ_2 and μ_3.

In order to track along the multiple solution branches which intersect at μ_n, we numerically computed the tangent direction for each solution branch. Since the Jacobian matrix is singular at μ_n, the double precision arithmetic in Matlab was unable to accurately compute these tangent directions. By using multiprecision arithmetic implemented in Bertini[2], we were able to compute the tangent directions which agreed with the symbolic formulas. Upon computing the tangent direction, we utilized parameter continuation to track the non-radially symmetric solution branches passing through μ_2 and μ_3 computed above. Figure 3.2 shows the solution behavior of these branches which were computed using $N_R = N_\theta = 20$. For this figure, the function $\epsilon(\mu)$ is defined as the difference between $\max_\theta r(\theta, \mu)$ and $\min_\theta r(\theta, \mu)$. It is positive if $\min_\theta r(\theta, \mu)$ is reached first as θ goes from 0 to π and negative if $\max_\theta r(\theta, \mu)$ is reached first as θ goes from 0 to π , i.e.,

$$\epsilon(\mu) = (r(\overline{\theta}, \mu) - r(\underline{\theta}, \mu)), \tag{3.2}$$

where $\overline{\theta} \geq \underline{\theta}$ are value on which $\max_\theta r(\theta, \mu)$ and $\min_\theta r(\theta, \mu)$ are reached respectively. Figures 3.3–3.6 present a non-radially symmetric solution on each of these four non-radially symmetric solution branches showed in Figure 3.2.

4. The model without symmetry. It is known [12] that the non-radial solutions near the bifurcation point μ_n has a symmetry property. We will track non-radial symmetry branches corresponding to the condition number of the Jacobian for the system without symmetry and check if there exists another bifurcation in this section. Since the system (1.7) is clearly translational and rotational invariant, the system has five degrees of freedom from translations and rotations by removing the symmetry assumption. The coordinates (x, y, z) of the origin yield the three degrees of freedom from translations. Rotations in θ and ϕ yield two degrees of freedom. This corresponds to the Jacobian of our discretized system having corank 5, which was verified numerically.

Since we are only concerned about the families of solutions, we center the domain at the origin, fix the x-axis as parallel to the normal direction at $\theta = \pi/2, \phi = 0$, and fix the y-axis as parallel to the normal direction at $\theta = \pi/2, \phi = 3\pi/2$. By fixing these choices, our Jacobian is full rank at solutions for a generic point μ.

To verify that the non-radially symmetric solution branches have this ϕ symmetry, we utilized this discretized system which did not impose this ϕ symmetry. The corank

of this Jacobian is also 1 at the critical points of μ_2 and μ_3 and the nonradially solution branches are the same as obtained before. No more bifurcation points are found by checking the condition number of the Jacobian for the system without symmetry along the non-radially symmetrical branches.

The left picture of Figure 4.1 displays the grid corresponding to a radially symmetric solution and the right picture of Figure 4.1 is the projection of the grid points onto the x, z plane.

5. Linear stability. Similar to [17], the linearized system of (1.7) is

$$
\begin{cases}
\sigma_{1t} - \Delta\sigma_1 + \sigma_1 = 0, & \text{in } \Omega_0 \\[2mm]
\quad -\Delta p_1 = \mu\sigma_1, & \text{in } \Omega_0 \\[3mm]
\sigma_1|_{r=\rho_0} = -\rho_1\sigma_{0r}|_{r=\rho_0} \\[2mm]
p_1|_{r=\rho_0} = \kappa_1 - \rho_1 \cdot p_{0r}\ |_{r=\rho_0} \\[2mm]
\rho_{1t}|_{r=\rho_0} = \left[\dfrac{p_{0r}\rho_{0\theta}}{\rho_0^2 + \rho_{0\theta}^2} + \dfrac{p_{0\theta}}{\rho_0^2 + \rho_{0\theta}^2}\right]\rho_{1\theta} + \left[\dfrac{p_{1\theta}\rho_{0\theta}}{\rho_0^2} - p_{1r}\right] \\[4mm]
\quad + \left[-\dfrac{p_{0r}\rho_{0\theta}^2}{\rho_0(\rho_0^2 + \rho_{0\theta}^2)} - p_{0rr} + \dfrac{p_{0\theta r}\rho_{0\theta}}{\rho_0^2} - \dfrac{p_{0\theta}\rho_{0\theta}}{\rho_0^3} - \dfrac{p_{0\theta}\rho_{0\theta}}{\rho_0(\rho_0^2 + \rho_{0\theta}^2)}\right]\rho_1
\end{cases}
\tag{5.1}
$$

Let $U^n = (\sigma_1(n\tau), p_1(n\tau), R_1(n\tau))$, where τ is the time step size. We solved the linearized system using a third order scheme in the spatial direction coupled with the backward Euler scheme in the time direction, which is unconditional stable. In particular, at every time-step, we solved the linear system $U^{n+1} = AU^n$, where the matrix A depends on σ_0, p_0, R_0 and τ.

This scheme transfers the question of linear stability to a question regarding the spectrum of the matrix A. In particular, if $|\rho(A)| < 1$, then $\|U^n\| \to 0$ which yields linear stability. Otherwise, it is linearly unstable. Tables 5.1 and 5.2 list the maximum absolute value of the eigenvalues of the matrix A for different values of μ along all the non-radially symmetric solution branches as in Figure 3.2.

6. Nonlinear stability. We now turn our attention to numerically determine nonlinear stability. To that end, let $G := r - R(\theta, \phi) = 0$ be the equation describing the boundary. Then, the velocity V_n of $\partial\Omega(t)$ is

$$
V_n = \frac{G_t}{\|\nabla G\|} = \frac{r_t r}{\sqrt{r^2 + R_\theta^2 + R_\phi^2/sin(\theta)^2}}
$$

Time marching with the system (1.6) allows us to numerically determine the local stability of the nonradial steady state solutions. In particular, we used a random perturbation of a solution as the initial condition as then computed the steady state solution. Our tests utilized a perturbation size on the order of 10^{-3}.

For example, consider the solution corresponding to $\mu = 3.9422$ on the "upper" solution branch. Table 5.1 yields that this solution is linearly stable. Figure 6.1 shows the convergence of the perturbed solution back to the original solution we

Table 5.1: Maximum eigenvalue for the "upper" branches in Figure 3.2

μ	$\max_{|\rho|}$	μ	$\max_{|\rho|}$	μ	$\max_{|\rho|}$
9.30460	1.0003895	8.49450	1.0003473	4.02897	0.9999995
9.22571	1.0003862	8.21950	1.0003308	3.92597	0.9999953
9.14521	1.0003825	7.94450	1.0003136	3.82297	0.9999911
9.06471	1.0003786	7.66950	1.0002958	3.71997	0.9999871
8.98421	1.0003745	7.39450	1.0002775	3.61697	0.9999834
8.90371	1.0003703	7.11950	1.0002589	3.51397	0.9999801
8.82321	1.0003660	6.84450	1.0002399	3.41097	0.9999773
8.74271	1.0003615	6.56950	1.0002206	3.30797	0.9999750
8.66221	1.0003570	6.29450	1.0002013	3.20497	0.9999732
8.58171	1.0003524	6.01950	1.0001824	3.10197	0.9999720

Table 5.2: Maximum eigenvalue for the "lower" branches in Figure 3.2

μ	$\max_{|\rho|}$	μ	$\max_{|\rho|}$	μ	$\max_{|\rho|}$
9.30996	1.0003897	7.99500	1.0002553	4.43128	1.0000753
9.21539	1.0003860	7.24500	1.0002989	4.43082	1.0000737
9.08177	1.0003776	6.49500	1.0003061	4.43169	1.0000745
8.94815	1.0003658	5.74500	1.0002070	4.39295	1.0000637
8.81453	1.0003514	4.99500	1.0002009	4.33595	1.0000521
8.68091	1.0003354	4.35318	1.0000877	4.27895	1.0000413
8.54729	1.0003185	4.38048	1.0000777	4.22195	1.0000309
8.41367	1.0003014	4.40151	1.0000771	4.16495	1.0000208
8.28005	1.0002846	4.41662	1.0000768	4.10795	1.0000111
8.14643	1.0002687	4.42651	1.0000762	4.05095	1.0000016

perform time marching in t using (1.6). In particular, this shows that this nonradially symmetric solution is stable.

We performed similar computations to yield the stability of the solution branches which is displayed in Figure 6.2. In particular, green lines denote the stable solutions and red lines denote the unstable solutions. Therefore, we have numerically verified that the non-radially symmetric solutions are stable for $\mu < \mu_2$ and unstable for $\mu > \mu_2$.
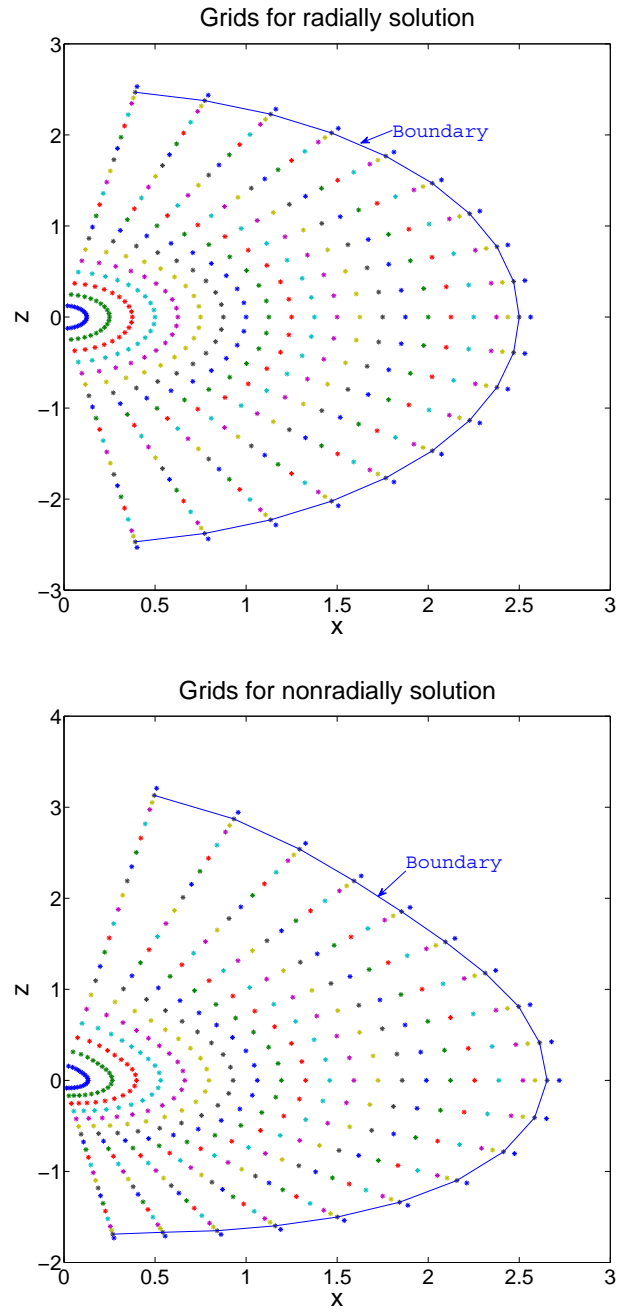
Fig. 2.2: Grid points
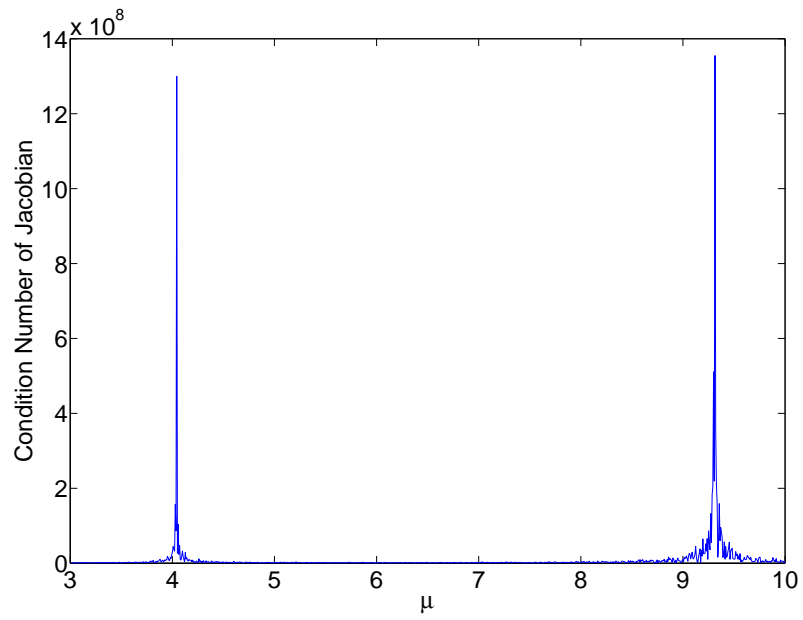
Fig. 3.1: Condition Number Tracking

Fig. 3.2: Solution Behavior

(a) Projection onto x, z plane

(b) Three dimensional picture
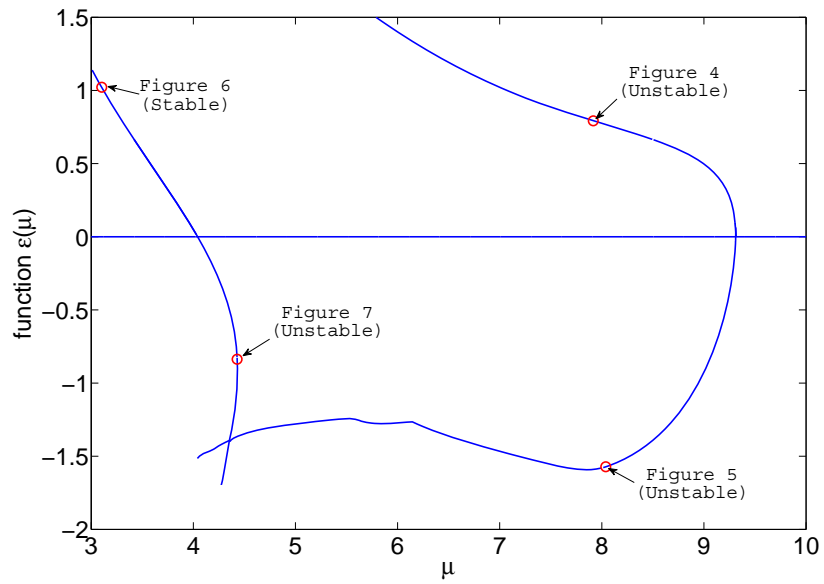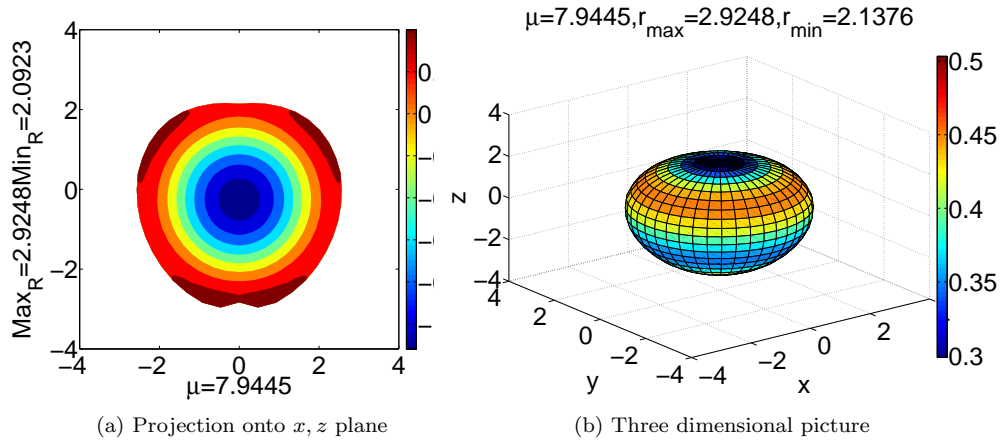
Fig. 3.3: $\mu = 7.9445$ on the upper branch

(a) Projection onto x, z plane

(b) Three dimensional picture
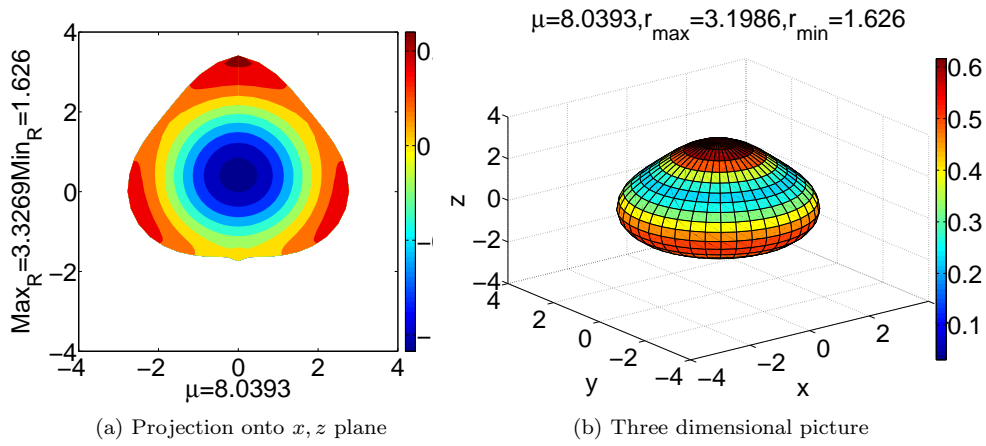
Fig. 3.4: $\mu = 8.0393$ on the lower branch

(a) Projection onto x, z plane

(b) Three dimensional picture
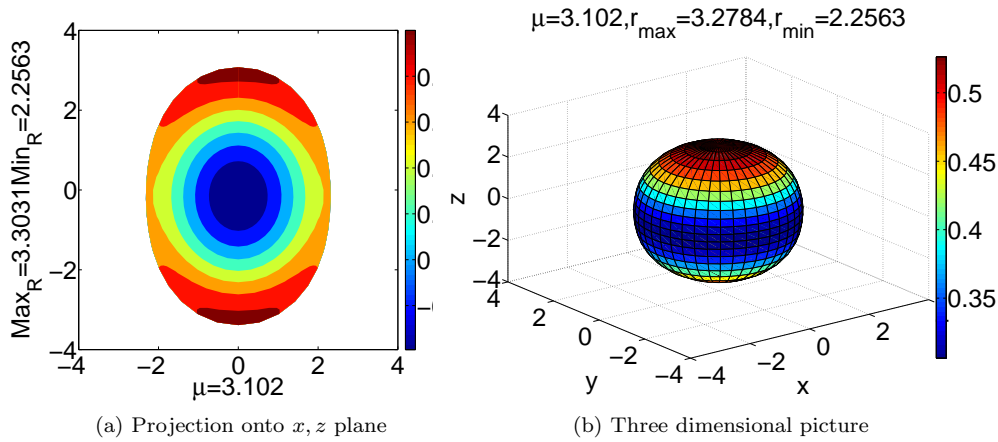
Fig. 3.5: $\mu = 3.102$ on the upper branch

(a) Projection onto x, z plane

(b) Three dimensional picture
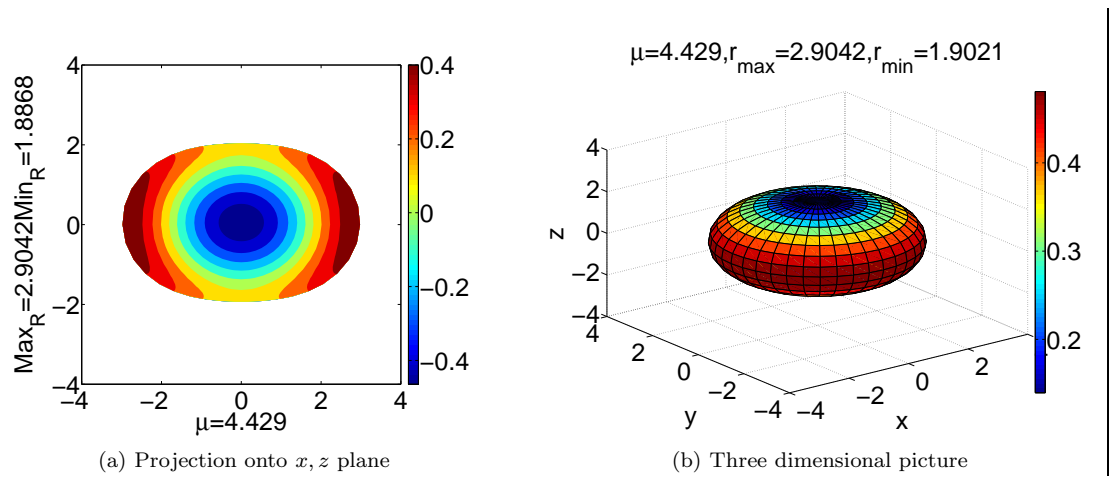
Fig. 3.6: $\mu = 4.4291$ on the lower branch
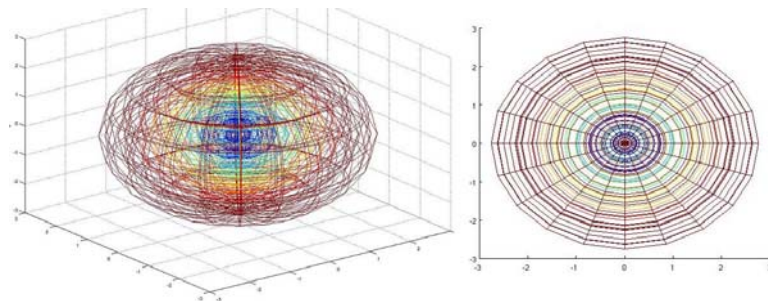
Fig. 4.1: Grid points without symmetry
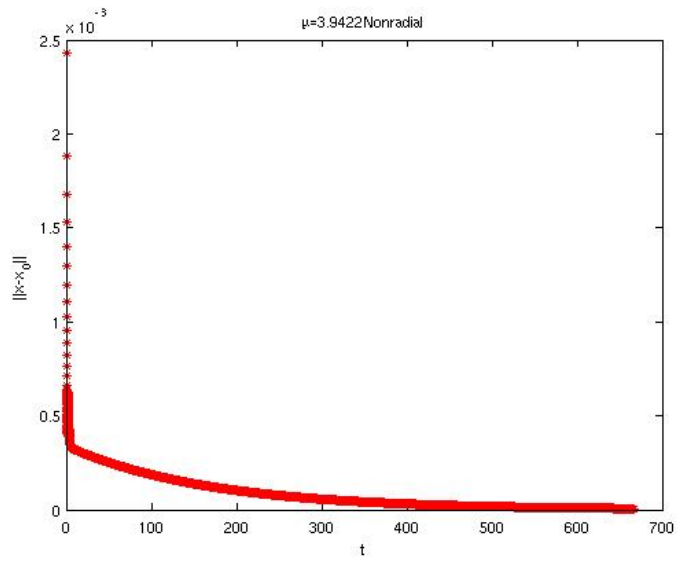
Fig. 6.1: Convergence of the perturbed nonradially symmetric solution at $\mu = 3.9422$
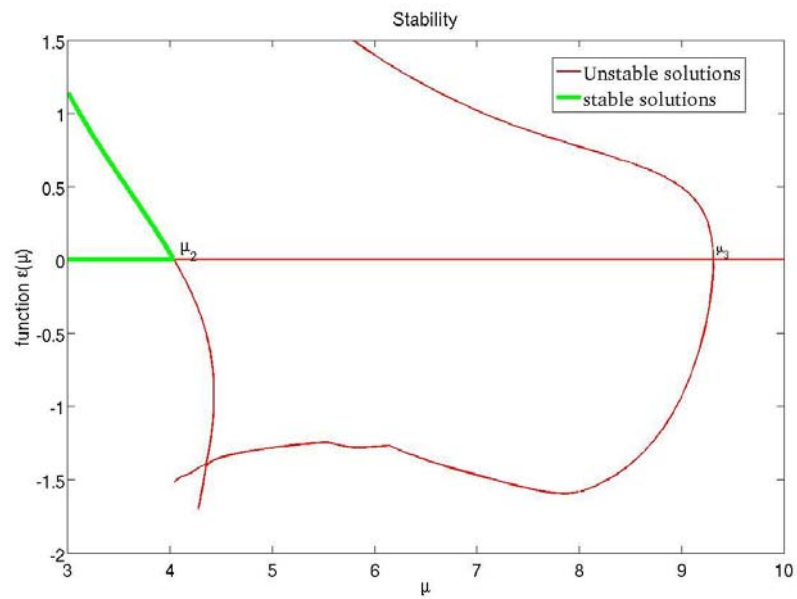
Fig. 6.2: Stability of the solutions

REFERENCES

[1] J.A. ADAM, General aspect of modeling tumor growth and immune response, A Survey of Models for Tumor-Immune System Dynamics (J.A.Adam and N. Bellomo, eds.) Birkhäuser, Boston, 14-87, (1996).

[2] D.J. BATES, J.D. HAUENSTEIN, A.J. SOMMESE, AND C.W. WAMPLER, Bertini: Software for numerical algebraic geometry. Available at www.nd.edu/∼sommese/bertini.

[3] B. BAZALLY AND A. FRIEDMAN, A free boundary problem for elliptic-parabolic system: Application to a model of tumor growth. *Comm. Partial Diff. Eq.* Vol 28, 517-560, (2003).

[4] B. BAZALLY AND A. FRIEDMAN, Global existence and asymptotic stability for an elliptic-parabolic free boundary problem: an application to a model of tumor growth. *Indiana Univ. Math. J.* 52, 1265-1304, (2003).

[5] N. BRITTON AND M.A.J. CHAPLAIN, A qualitative analysis of some models of tissue growth, *Math. Biosci.*, Vol 113, 77-89, (1993).

[6] H.M. BYRNE, The importance of intercellular adhesion in the development of carcinomas, *IMA J. Math. Appl. Med. Biol.*, Vol 14, 305-323, (1997).

[7] H.M. BYRNE, A weakly nonlinear analysis of a model of avascular solid tumor growth, *J. Math. Biol.*, Vol 39, 59-89, (1999).

[8] H.M. BYRNE AND M.A.J. CHAPLAIN, Growth of nonnecrotic tumors in the presence and absence of inhibitors, *Math. Biosci.*, Vol 130, 151-181, (1995).

[9] H.M. BYRNE AND M.A.J. CHAPLAIN, Modelling the role of cell-cell adhesion in the growth and development of carcinomas, *Mathl. Comput. Modelling*, Vol 12, 1-17, (1996).

[10] M. FONTELOS AND A. FRIEDMAN, Symmetry-breaking bifurcations of free boundary problems in three dimensions, *Asymptotic Analysis*, Vol 35, 187-206, (2003).

[11] A. FRIEDMAN AND B. HU, Bifurcation from stability to instability for a free boundary problem arising in a tumor model *Arch. Rat. Mech. Anal.*, Vol. 180, No. 2, (2006).

[12] A. FRIEDMAN AND B. HU, Stability and instability of Liapunov-Schmidt and Hopf bifurcation for a free boundary problem arising in a tumor model. *Trans. Amer. Math. Soc.*, Vol 360, 5291–5342, (2008).

[13] A. FRIEDMAN AND F. REITICH, Analysis of a mathematical model for growth of tumor, *J. Math. Biology*, Vol 38, 262-284, (1999).

[14] A. FRIEDMAN AND F. REITICH, Symmetry-breaking bifurcation of analytic solutions to free boundary problems: An application to a model of tumor growth. *Trans. Amer. Math. Soc.*, Vol 353, 1587-1634 (2000).

[15] H.P. GREENSPAN, Models for the growth of a solid tumor by diffusion, *Studies Appl. Math*, Vol 52, 317-340, (1972).

[16] H.P. GREENSPAN, On the growth of cell culture and solid tumors, *Theoretical Biology*, Vol 56, 229-242, (1976).

[17] W. HAO, J.D. HAUENSTEIN, B. HU, Y. LIU, A.J. SOMMESE, AND Y.-T. ZHANG, Bifurcation of steady-state solutions for a tumor model with a necrotic core, preprint available at *http://www.nd.edu/∼sommese/preprints*.